Article

Mobile LiDAR System: New Possibilities for the Documentation and Dissemination of Large Cultural Heritage Sites

Pablo Rodríguez-Gonzálvez [1],*, Belén Jiménez Fernández-Palacios [1], Ángel Luis Muñoz-Nieto [1], Pedro Arias-Sanchez [2] and Diego Gonzalez-Aguilera [1]

[1]   TIDOP Research Group, University of Salamanca, Polytechnic School of Avila. Hornos Caleros, 50, 05003 Avila, Spain; belenjfp@gmail.com (B.J.F.-P.); almuni@usal.es (Á.L.M.-N.); daguilera@usal.es (D.G.-A.)
[2]   Department of Natural Resources & Environmental Engineering, University of Vigo, School of Mining Engineering, Maxwell s/n, 36310 Vigo, Spain; parias@uvigo.es
*   Correspondence: pablorgsf@usal.es; Tel.: +34-920-353-500

Abstract: Mobile LiDAR System is an emerging technology that combines multiple sensors. Active sensors, together with Inertial and Global Navigation System, are synchronized on a mobile platform to produce an accurate and precise geospatial 3D point cloud. They allow obtaining a large amount of georeferenced 3D information in a fast and efficient way, which can be used in several applications such as the 3D recording and reconstruction of complex urban areas and/or landscapes. In this study the Mobile LiDAR System is applied in the field of Cultural Heritage aiming to evaluate its performance with the purpose to document, divulgate, or to develop an architectural analysis. This study was focused on the Medieval Wall of Avila (Spain) and, specifically, the performed accuracy tests were applied in the "Alcazar" gate (National Monument from 1884). The Mobile LiDAR System is then compared to the most commonly employed active sensors (Terrestrial Laser Scanner) for large Cultural Heritage sites in regard to time, accuracy and resolution of the point cloud. The discrepancies between both technologies are established comparing directly the 3D point clouds generated, highlighting the errors affecting the architectural structures. Consequently, and based on a detailed geometrical analysis, an optimization methodology is proposed, establishing a segmented and classified cluster for the structures. Furthermore, three main clusters are settled, according to the curvature: (i) planar or low curvature; (ii) cylindrical, mild transitions and medium curvature; and (iii) the abrupt transitions of high curvature. The obtained 3D point clouds in each cluster are analyzed and optimized, considering the reference spatial sampling, according to a confidence interval and the feature curvature. The presented results suggest that Mobile LiDAR System is an optimal approach, allowing a high-speed data acquisition and providing an adequate accuracy for large Cultural Heritage sites.

Keywords: cultural heritage; mobile LiDAR system; point cloud; terrestrial laser scanner; accuracy assessment; optimization

1. Introduction

Recent advances in Geomatics Science enable the use of a wide range of sensors to record, catalogue and analyze Cultural Heritage (CH) sites: from RGB and multispectral cameras [1,2] and Terrestrial Laser Scanner (TLS) [3], to Ground Penetrating Radar (GPR) [4] and Raman Spectroscopy [5]. Furthermore, airborne LiDAR (Laser Imaging Detection and Ranging) is used as a remote sensing device for 3D surveying and modeling of extensive archaeological sites [6,7]. Nowadays, hybrid

sensors such as Mobile LiDAR Systems (MLS) [8,9] bring added value to record large and complex sites. Although the most common solution based on MLS are boarded on vans and applied in the field of civil engineering and construction [10], MLS has been useful in other fields, such as geology [11]; agriculture, biology or forestry [12–14]; and even in the inspection of high-voltage power lines [15]. The last developments allow the use of MLS boarded in a backpack [16] or even in autonomous robots [17], offering a flexible solution in terms of accuracy, flexibility, point density and access to indoor and non-transitable areas [18–22]. These specific solutions are still under development and several approaches are being experienced and tested [23,24].

MLS process and management optimization has become a key point. Even though MLS reduces extremely data collection phase, it still requires a lot of time and resources consumption to extract meaningful information [25] and even more time for 3D modeling. At this point, and for large and unstructured point cloud, some authors [26] showed that it is more efficient to carry out the simplification of the point cloud before creating a mesh. In terms of workflow optimization, it may be useful when the presence of particular characteristics (e.g., breaklines) is desirable [27]. MLS optimization, understood not only as decimation but a smart filtering, has proven to be relevant in different fields, such as infrastructures management [28], reverse engineering [29], object detection [30], object fitting [31] and visualization optimization through Web services by means of mobile devices [32].

It is a well-known fact that CH information systems such as Nubes Project [33,34] and Cultural Heritage Information System Projects [35–37] become the basis for an effective management of CH. However, they are also extremely important for its dissemination and decision making. These Systems and Projects are usually based on 3D Web interfaces [38]. Thus, it is clear that, in order to guarantee and improve the specific visualization requirements of 3D Web systems, the MLS complex geometric datasets need to be optimized.

Based on the remarks above, this paper aims to analyze the suitability of MLS for CH documentation and dissemination purposes from a two-fold approach. Firstly, an accuracy assessment is performed. For this purpose, the acquired MLS data were compared with a ground truth defined by a milimetric laser scanner point cloud. Secondly, the data suitability, in terms of 3D point cloud optimization for the data dissemination, is evaluated.

This manuscript is organized as follows. After the Introduction, sensors and devices are described in Section 2. In Section 3, the multi-sensor integration methodology and multi-data process workflow proposed are detailed. In Section 4, the representative study case of the Medieval Wall of Avila (Spain) is shown. Finally, in Sections 5 and 6, discussion and conclusions are respectively discoursed.

2. Materials

The evaluated mobile LiDAR technology is a LYNX Mobile Mapper manufactured by Optech (Figure 1) [9,39]. This system is composed of two LiDAR sensors, four RGB cameras and an Applanix POS LV 520 IMU. The system is configured to take 500,000 points per second with a scan frequency of 200 Hz. The maximum range of the sensors is 200 m, with a precision of 8 mm (one sigma) and permission to obtain up to 4 echoes of the signal and the intensity reflected by the objects at a 1550 nm wavelength (Table 1). Along with the geometric measurement system, the MLS incorporates a multisensory camera to acquire the radiometric texture of the scanned elements.

In this study, the MLS is mounted on a car, achieving speeds up to 40 km/h during the data capture.

Figure 1. LYNX Mobile Mapper manufactured by Optech.

Table 1. Technical specifications of Optech LYNX Mobile Mapper.

MLS Technical Parameters	
X, Y position	0.020 m
Z position	0.050 m
Roll and pitch	0.005°
True heading	0.015°
Measuring principle	Time of Flight (ToF)
Maximum range	200 m
Range precision	8 mm (1σ)
Range accuracy	±10 mm (1σ)
Laser measurement rate	75–500 kHz
Measurement per laser pulse	Up to 4 simultaneous
Scan frequency	80–200 Hz
Laser wavelength	1550 nm (near infrared)
Scanner field of view	360°
Operating temperature	10–40 °C
Angular resolution	0.001°

The use of MLS is not completely straightforward. It requires an initial data acquisition plan, especially for the large cultural heritage sites. In this regard, any error in the INS will be directly propagated to the point cloud, being especially complicated in scenarios with the presence of narrow streets (e.g., urban CH sites), or dense vegetation, which could provide a loss in accuracy by the multi-path and occlusion of the GNSS signal [40]. Besides, the boresight angles and level-arm (related to the MLS assembly), which are kept constant throughout the whole scanning process, require to be precisely determined to avoid any loss in the overall accuracy [41]. To this end, some regular surfaces (e.g., road surface) should be measured prior to the data acquisition for its calibration. The most critical aspect in data acquisition planning is the boresight, which could cause that same scene acquisition in different trajectories to not overlap correctly. Additionally, the height of the CH buildings could be a limitation to the system due to the vertical angle, so those trajectories closer to the object should be avoided to reduce the occlusions in the final point cloud.

To assess the quality of the MLS, a Time-of-Flight (ToF) [42,43] TLS Trimble GX is employed, found on direct time measurement. It is typically more precise than the phase-shift (PS) ones [43,44], for instance, measurement amplitude-modulated continuous wave method (AMCW) based on indirect time, with lower range but further point acquisition speed. The main technical specifications are shown in Table 2. In a ToF System, the distance to the surface and the position of the points (X, Y, Z) are calculated from the time of the flight of the pulse; a laser pulse is emitted towards the object and, once it is reflected from the object surface, returns to the equipment. The distance to the object can be determined by half of the round-trip range. Nowadays, both technologies are competing;

PS technology increasing its range, while ToF technology improving the acquisition speed. Regarding the TLS accuracy evaluation, please refer to [45,46].

Table 2. Technical specifications of the Trimble GX laser scanner.

TLS Technical Parameters	
Measuring principle	Time of Flight (ToF)
Laser wavelength	534 nm (visible-green)
Scanner field of view	360° H × 60° V
Range precision	1.4 mm at 50 m
Measurement range	2–350 m
Spot size (beam diameter)	3 mm a 50 m
Scanning speed	5000 points/sec

In order to georeference the TLS point cloud in a global coordinate reference system (ETRS89) 50 GPS control points were acquired. The GPS points, well distributed through the entire area of interest, were surveyed using two Leica 1200 GPS. This device is a dual frequency receiver which was used with Real Time Kinematic (RTK) method. The a-priori precision of this measurement method is 1 cm in horizontal plane and 2 cm in vertical axis.

3. Methods

In this section the two geomatics techniques employed, as well as the specific assessment methodology and the developed algorithms for the optimization of point clouds, are described. In Figure 2 the global pipeline for the geometric accuracy and optimized assessment data aimed at 3D web visualization and dissemination is shown.
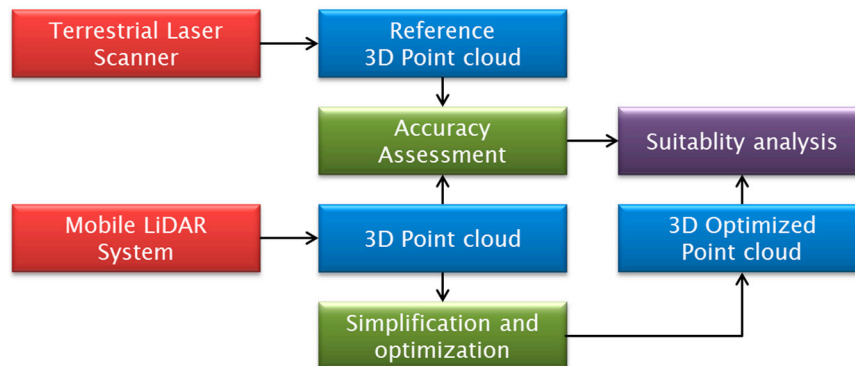

Figure 2. Pipeline for the assessment of Mobile LiDAR Systems (MLS) for Cultural Heritage recording and modeling.

3D data acquired by active sensors (TLS and MLS) are processed following a conventional workflow. In the case of TLS, the obtained unstructured point clouds (individual scans) are cleaned, edited and aligned in a common local reference system. The alignment process can be automatically carried out through Iterative Closest Point (ICP) points [47], by automatic recognition of objects [48] or using artificial targets [49]. The 3D point cloud obtained with milimetric resolution can include the intensity levels (I) and/or the color information (RGB). Finally, the aligned point cloud is georeferenced in a global reference system by means of targets of known coordinates. Regarding the MLS, three main types of sensors take part in data acquisition using three independent reference systems. A multi-sensor calibration is mandatory to determine the translational and rotational offsets among the different sensors and bring all the data into the same reference system [50]. As a result, the unstructured point cloud is already aligned in a global reference system by means of the navigation/positioning sensors with centimetric absolute precision (typically). The 3D point cloud obtained uses to have also

a centimetric resolution, including at least the intensity levels of returned pulses or even the color information (RGB).

3.1. Accuracy Assessment Protocol

Since the MLS involves several sensors (e.g., IMU, LiDAR, GNSS, etc.) to acquire a georeferenced 3D point cloud, the aim of this step is to analyze, in the CH field, the quality of the MLS point cloud using a ground truth provided by a TLS. To dismiss the uncertainties associated to the global coordinate geo-referencing, a registration phase with the Iterative Closest Point (ICP) technique is carried out, prior to the MLS point cloud evaluation [51]. As a result, only those errors affecting the 3D point cloud of the architectural elements are analyzed. Particularly, discrepancies are computed in consonance with Multiscale Model to Model Cloud Comparison (M3C2) [52], which performs a direct comparison of the 3D point clouds (TLS to MLS), avoiding the preliminary phase of meshing.

In order to prevent possible bias effects affecting the data processing, the normality assumption, i.e., the hypothesis that errors follow a Gaussian distribution, are checked according to graphical methods such as QQ-plot [53] well-suited for very large samples [54]. If the samples are not normally distributed, either due to the presence of outliers or because of a different population hypothesis, a robust model based on non-parametric estimation should be employed. In this case, the median (m) and the median absolute deviation (MAD) are used as robust measures instead of the mean and standard deviation, respectively. The MAD is defined as the median (m) of the absolute deviations from the data's median (m_x):

$$MAD = m(|x_i - m_x|) \tag{1}$$

where the x_i values come from the discrepancies (Euclidean distance) between both point clouds (TLS and MLS).

The computation of the discrepancies maps is carried out by Cloud Compare v2.7.0 software [55], being a point cloud-to-point cloud based on the M3C2 plugin [52]. The robust statistical estimators are computed by a custom script as well as the in-house statistical software (STAR (Statistics Tests for Analyzing of Residuals)) [56].

3.2. Point Cloud Optimization

Despite recent technological breakthroughs, it is still common to face some limitations since 3D datasets obtained by active sensors (TLS and MLS) produce complex reality-based 3D point clouds which are generally large. For extensive CH sites, the geometric component hinders the access for analysis purposes through Web visualization, worsen when mobile devices (e.g., tablets or smartphones) are used, due to the vast amount of information. Depending on the device used and the size of the 3D models, a delay might occur that could affect the fluidity of the 3D scene. Moreover, the 3D point cloud acts as mainframe for the extraction of semantic and/or vector information, avoiding the meshing step. The common algorithms used to generate a mesh are time-consuming, since they require human intervention to correct topological errors (e.g., non-manifold edges, loose edges, overlapping faces, self-intersections, etc.) that could be generated, and the holes filling required to rebuild those areas affected by errors and occlusions. Thus, different simplification and optimization strategies would be desirable to be applied to the 3D point clouds, while keeping the relevant information for the subsequent studies and/or operations in the global pipeline of CH conservation and management.

The proposed optimization methodology (Figure 3) is based on an idealization process and an adaptive sampling according to a confidence interval and local feature curvature. Thus, the more significant are the points, the more 3D points are kept to represent those complex areas of the site. On the contrary, for those parametric and simple geometrical CH elements such as planes, the point cloud is considerably reduced in size.

The point cloud optimization strategy has been developed following three global phases: (i) a preparation phase to setup the raw point cloud acquired from MLS; (ii) a clustering phase based on a curvature segmentation; and (iii) a final weighted sampling phase.
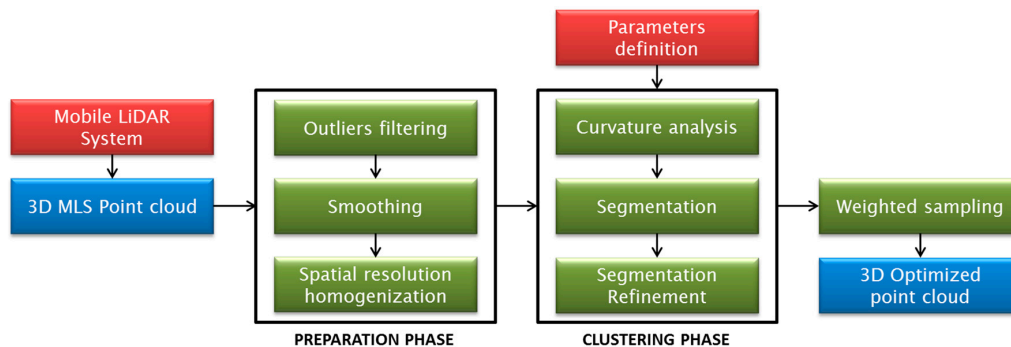

Figure 3. Pipeline for 3D point cloud optimization.

The *preparation phase* involves three sub steps in the following order:

- An initial outliers filtering of the MLS point cloud based on the absolute deviation (Euclidean distance) of the points from a fitted local plane in a spherical vicinity. The absolute threshold is not set very strictly to avoid false positives. In the case a plane cannot be fitted in the neighborhood, the point is also excluded.
- Next, in order to ease the simplification, a local smoothing process by means of a moving least squares [57] is applied. This operation involves a point displacement regarding the original positions; however, the spherical search volume is chosen in relation to the precision obtained from the accuracy assessment studies (see Section 3.1) to avoid a precision deterioration of the final optimized point cloud.
- Finally, a reduction of high point density areas, due to the MLS acquisition methodology, is applied. For this task, a spatial sampling is carried out. The sampling value determines the final results. Since there are several options for this sampling value, all of them being related to the input point cloud precision, the proposed one is to setup the 95% confidence interval of the error dispersion from the accuracy assessment studies. By this procedure, it is possible to guarantee the optimized final results.

Once the point cloud is ready, the *curvature clustering* phase is carried out following the next three sub steps:

- Initially, the local curvature is computed in a wide spherical neighborhood to reduce noise effects. The spherical radius for the curvature calculation is defined in relation to the main geometrical elements of the CH site (i.e., a-priori length and height).
- Next, the 3D point cloud is segmented according to the computed local curvature and the a-priori approximate knowledge of the main geometrical primitives presented (e.g., planes and radius of cylinders). These coarse values allow defining a discrete number of clusters according to a similar curvature values. The final number of clusters is increased in one, since the highest curvature values are related to non-parametric areas, as the break-lines, borders, corners, abrupt areas, surface discontinuities or geometric and topological errors.
- Finally, since the curvature computation and clustering could be affected by local errors, especially in transition areas, a refinement based on connected component analysis is carried out to reclassify them in the more suitable cluster. This analysis is based on an octree representation of the point cloud, so a reference subdivision level has to be set. In order to find connected components, the octree level has to be set slightly higher than the homogenized spatial resolution. Since the

spatial resolution was homogenized in the *preparation phase*, and an octree level has to be fixed, it is possible to relate easily the component's area by the number of points. For the main features of the CH site, it is possible to define their minimum area. As result, the components inside a cluster that do not verify this minimum area are reallocated to the neighbor cluster in crescent curvature. No points are removed.

Lastly, a *weighted sampling* is applied to all the points inside a cluster based on the associated feature (e.g., plane, cylinder, etc.) and based on the maximum and minimum curvature values of the cluster. The highest curvature cluster is kept unmodified, since encloses all the conflictive areas. The others cluster thresholds, low and medium curvature, are established according to its geometric elements. For instance, the number of points of a wall could be drastically reduced if points can be assimilated/idealized as a plane. In the cases of other elements as towers, the arc to chord approximation was used. Thus, a final 3D optimized point cloud is obtained, retaining all the geometrical relevant information for subsequent tasks, as vectorization, reverse engineering, finite element (FEM) analysis and information management through HBIM or even for Web visualization.

4. Experimental Results

The case study was the Medieval Wall of Avila. Its construction is the most important example of military architecture of the Spanish Romanesque style as well as an exceptional model of European medieval architecture [58]. The construction of the city wall is perfectly adapted to the topography. The wall was used not only to defend the town from possible invasions and protect the people from possible pests or epidemics, but also to control the trade of the city with the outside. The southern sectors are shorter as they are built upon a cliff that acts as a natural defense. The western and northern sections grow in height, reaching the tallest and thickest points located in the east section. There are nine gates giving access to the town, of which the most spectacular is "*Puerta del Alcázar*" (Gate of the Fortress). In 1884, it was declared a National Monument and in 1985, the old city of Ávila and its extramural churches were declared a World Heritage site by UNESCO. Some references state that the building dates back to 1090. Other researchers have argued instead that the wall's construction most likely continued through into the 12th century. Its large size is a clear example of a challenging CH sites for the recording and documentation processes. Despite its linear nature (Figure 4), the towers and wall distribution, the gates, and neighbor city buildings add difficulties for acquisition and processing. Since the case study presents a repetitive pattern (i.e., wall–tower–wall) along its whole extension, only a significant part of its extension was evaluated. Thus, the obtained results could be extrapolated to the whole medieval Wall. The main geometric information is shown in Table 3.

Table 3. Avila's Medieval Wall main dimensions.

Parameter	Value
Perimeter	2516 m
No. of towers	87
No. of Battlement elements (current/original)	2113/2379
No. of gates	9
Width of the wall	Between 2.6 and 2.8 m
Average height of the wall	11.5 m
Average height of the towers	15 m

The 3D point cloud of the whole medieval wall coming from the TLS was carried out using the process described in [59]. The spatial resolution achieved was 15 mm for an average scanning distance of 20 m. The georeferencing of the TLS into a global coordinate system (ETRS89) was done by a GNSS network of 50 control points, using two Leica 1200 GPS, distributed in the towers and the upper part of the wall as well as along its base. The registration errors of the individual TLS scans have been

evaluated by a network of control points, analyzing its propagation in a close object. The discrepancies reached up to 5 cm as stated in [59]. The TLS workload involved 159 h for the 2.5 km perimeter wall.

The 3D point cloud obtained (Figure 5) by means of MLS of the whole Medieval Wall of Avila was carried out according to the process described in [60]. The spatial resolution acquired was 60 mm for an average scanning distance of 25 m. The georeferencing of the LiDAR 3D point cloud into a global coordinate system was done by the integrated IMU sensor (Applanix POS LV 520) on the LYNX Mobile Mapper.
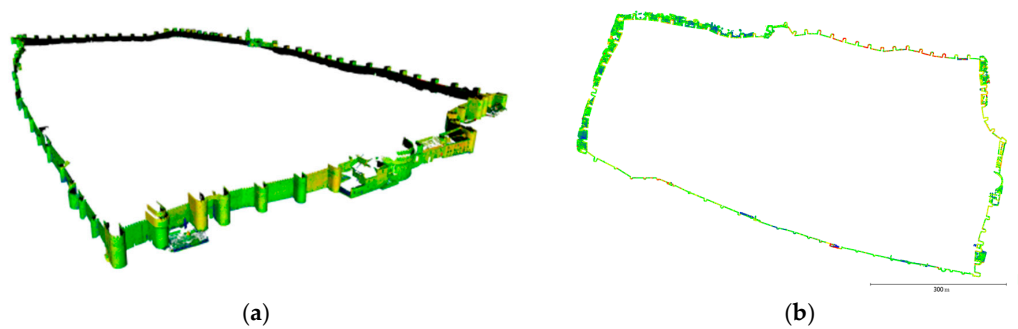

(**a**)　　　　　　　　　　　　　　　　　　　　(**b**)

Figure 4. TLS 3D point cloud (**a**); and *XY* view (**b**) of the Wall of Avila.

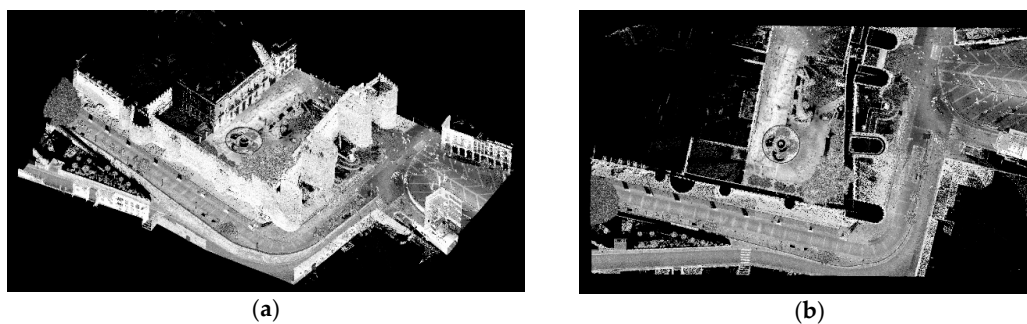(**a**)　　　　　　　　　　　　　　　　　　　　(**b**)

Figure 5. MLS 3D point cloud (**a**); and *XY* view (**b**) of the "Puerta del Alcázar" (Gate of the Fortress) of the Wall of Avila.

MLS and TLS workload, in terms of time consumption and accuracy, is compared in Table 4.

Table 4. Comparison between MLS and TLS field work and processed point cloud.

	Trimble GX	LYNX Mobile Mapper
Measuring principle	Time of Flight (ToF)	Time of Flight (ToF)
Range	350 m to 90% reflectivity 200 m to 35% reflectivity 155 m to 18% reflectivity	250 m to 10% reflectivity
Resolution	15 mm	60 mm
Scanning speed	up to 5000 points per second	up to 500 lines/sec
Scanned area (approximate)	30,000 m^2	250,000 m^2
No. of stations	98	1
No. of points	300,000,000	185,000,000
No. of images	215	420
Geodetic reference system-projection	ETRS89 and UTM30	ETRS89 and UTM30
Acquisition time	150 h (laser) + 4 h (camera) + 5 h (GNSS)	1 h
Processing time	435 h	15 h

4.1. Point Cloud Accuracy Assessment

The accuracy assessment was focused in the named "Alcazar" door, one of the highest wall entrances (Figure 6), and its vicinity, originally annex to the "Alcazar" fortress, where the defensive system was reinforced with a barbican and a ditch.
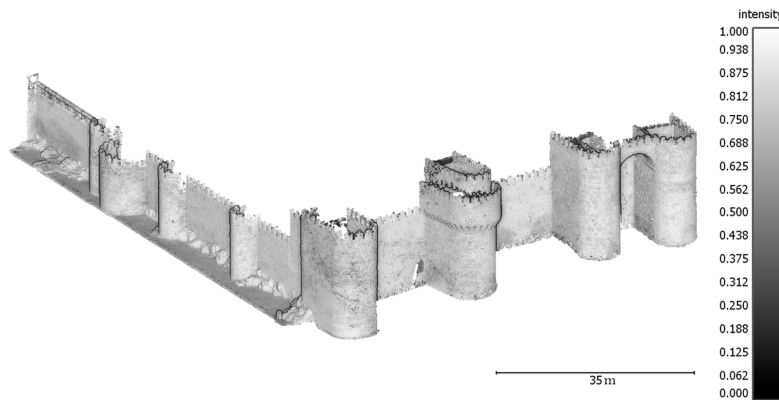

Figure 6. Segmented MLS point cloud of the analyzed zone (southeast walls), coded according to the intensity values.

The georeferencing error of the MLS is dependent on three factors: the GNSS system, the trajectory compensation and the calibration method of its sensors. The georeferencing error of the TLS is associated with the two GPS receivers used. Thus, in order to evaluate the accuracy of a MLS point cloud, a registration phase with ICP was carried out. Consequently, a comparison of both 3D point clouds was done (TLS and MLS). After the removal of the non-overlap areas (e.g., parts acquired by the MLS but not by the TLS), the discrepancies map was computed, as shown in Figure 7, separately for the east walls (Figure 7a) and the south walls (Figure 7c), which delimitated the fortress. These discrepancies were computed using the point cloud-to-point cloud comparison, obtained as the result of the signed error between both point clouds.
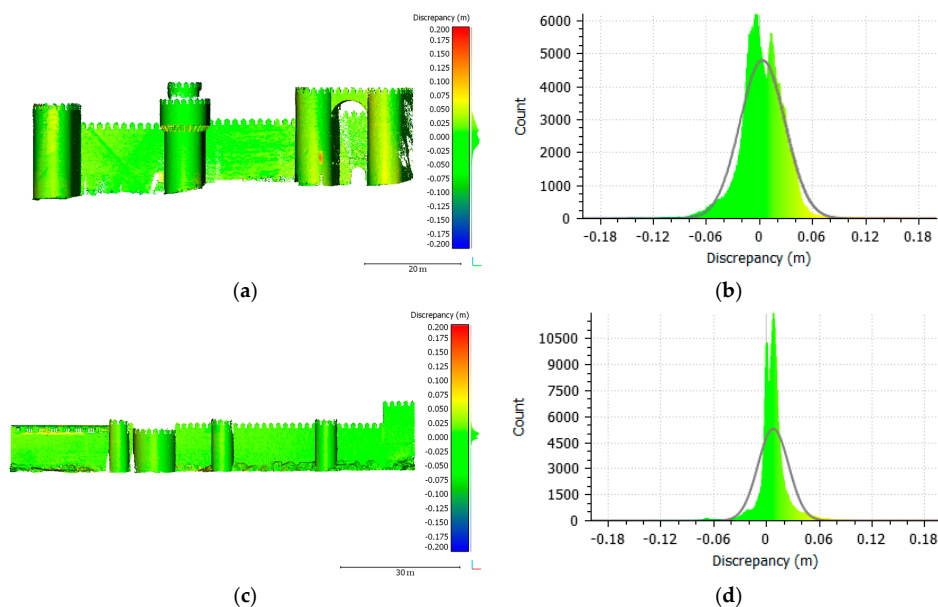

(a)

(b)

(c)

(d)

Figure 7. Relative discrepancies maps between MLS and TLS in the "Alcazar" fortress (**Left**) and its associated histogram (**Right**) for the: east walls (**a**,**b**); and south walls (**c**,**d**).

The obtained values were analyzed with a QQ-plot to confirm the non-normality of the sample (Figure 8). This fact was hinted by the histogram shape (Figure 7b,d), but since it is directly dependent on the bin size, it cannot be used as decision criterion. Since this sample does not follow a normal distribution (Figure 8), it is not possible to infer the central tendency and dispersion of the population according to Gaussian statistics parameters such as mean and standard deviation. For that reason, the accuracy assessment was computed based on robust alternatives, using non-parametric assumptions such as the median and the MAD value shown in Table 5.
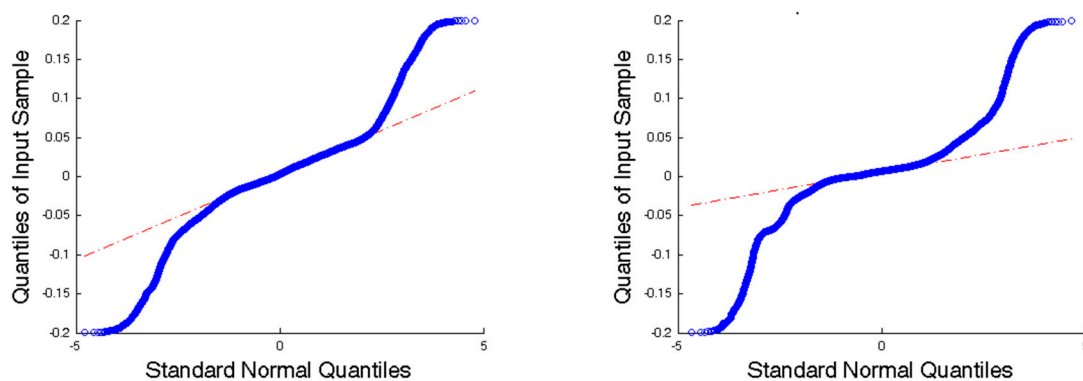

Figure 8. QQ-plots of relative discrepancies between MLS and TLS in the "Alcazar" fortress for the: east walls (**left**) and south walls (**right**).

Table 5. Robust statistical descriptors associated to relative discrepancies.

Statistics	Value		
	East	**South**	**Global**
Mean	0.003 m	0.008 m	0.005 m
Standard deviation	±0.026 m	±0.017 m	±0.023 m
Median	0.003 m	0.007 m	0.005 m
MAD	±0.015 m	±0.006 m	±0.011 m
Quantile 25	−0.011 m	0.000 m	−0.006 m
Quantile 75	0.019 m	0.013 m	0.016 m

In this analysis, the median value is close to zero (2.8 mm in the east wall), as was expected after the application of the ICP registration algorithm. However, a slightly higher value of 6.9 mm is appreciated in the south wall, which points to some registration error, but it is inside the expected range. Moreover, in Table 5, the dispersion value (MAD) is according to the expected error, confirming the MLS a-priori reference values, especially in the south wall, which has a simple geometry (Figure 7c). The analysis of the error sample by means of the non-parametric estimator for the quantile, yields that the 95% of the error points are inside the [−0.046 m; 0.047 m] interval. This reference value is used in the optimization phase to carry out the point cloud simplification.

It is worth noting that, despite the symmetrical shape of the sample in the east wall (as shown in the first and third quartile), there is a high difference (up to three times) between the standard deviation and the MAD having as reference the south wall. The conclusions would seem wrong without an adequate statistical parameter selection.

In conclusion, the spatial resolution achieved by the MLS and his distribution is directly related to the sensor–object distance; therefore, there will be areas with higher point density than others (Figure 9). Moreover, in Figure 9, some diagonal stripes are shown by cause of inhomogeneity in the acquisition phase due to the oblique laser scanner heads arrangement in the vehicle (Figure 1). This fact is not a critical issue, but reinforces the necessity of a 3D point cloud data optimization that copes with those redundant areas.
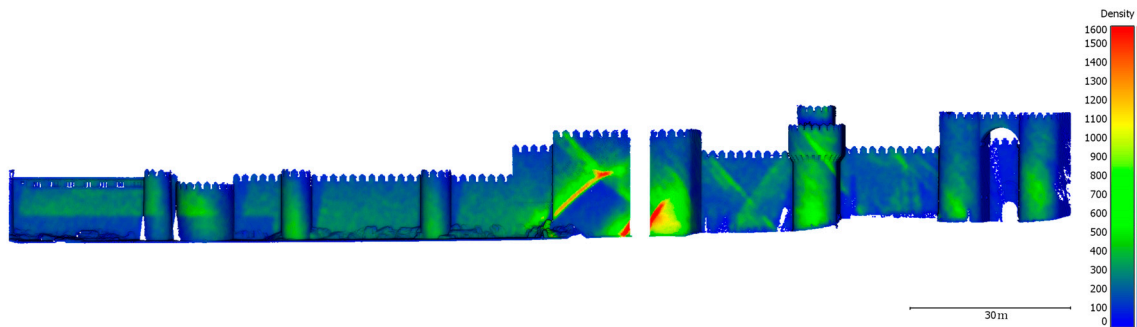
Figure 9. MLS point density distribution (points/m^2) for the southeast walls.

According to an ideal equilateral triangles distribution for a circular neighborhood [61], the average point density achieved is 58.8 mm, decreasing up to a spatial resolution of 135 mm for the farthest zones (e.g., battements and upper parts of towers). In addition, the occlusion in these zones underestimates the density computation since the point vicinity is incomplete.

4.2. Optimization Analysis

In the Medieval Wall of Avila, two main features are clearly recognized: the planar walls and the cylindrical towers. On the one hand, the walls are considered to have zero curvature, but due to the construction processes and the deterioration of the structures caused by the course of time, the actual conservation state does not keep this property. Therefore, a slight curvature of 0.005 m^{-1} (200 m radius) can be assumed. Additionally, the individual stones of the wall also contribute to local groups of higher curvature, so this threshold is extended to the annexed towers. On the other hand, in the case of the towers, the diameters of the cylinders range from 4.5 to 10 m. Accordingly, the upper limit for the curvature cluster is set as 0.4 m^{-1}. The rest of the elements (e.g., battlements, arrow slits or natural rocks) are contained in a final cluster of higher local curvature.

The size of these main elements (walls and towers) suggests a wide neighborhood for the computations to balance the curvature precision and noise effects. The minimum height of 10 m and the typical wall width of 20 m favors this large neighborhood. By a selection of a spherical diameter of 2 m for the curvature computation, implicitly, a security buffer of 1 m is kept between the different clusters. Additionally, a minimum area of 1 m^2 per cluster is set as threshold for the clustering refinement.

As the final parameter definition, the sampling interval for the homogenization is chosen as 5 cm, which, according to Section 4.1, is the nearest round value corresponding to the 95% non-parametric confidence interval of the MLS point clouds. In the first step of the *preparation phase*, 0.4% of points were excluded as outliers, since they exceeded the point to local plane distance of 20 cm. As result, after the smoothing process and the spatial resolution homogenization, 521,090 points were obtained, which implies a 47.4% reduction of the original input.

Next, the curvature analysis is carried out for a spherical neighborhood of 1 m of radius, which is segmented according the three pre-established clusters: (i) planar or low curvature (<0.05 m^{-1}); (ii) cylindrical, mild transitions and medium curvature (0.05–0.40 m^{-1}); and (iii) the abrupt transitions of high curvature (>0.40 m^{-1}). The results are outlined in Figure 10.

Subsequently, these clusters are refined based on a connected components analysis. The octree level is chosen in relation to a reference spatial sampling of 0.12 m, which corresponds to 160 points per square meter. Table 6 shows the percentage of reallocated components per cluster and the final classification. For the low curvature cluster, the main planar elements are coded by only 47 components, the rest being small components (about two thousand) located in the transition area of the wall planes, and in the transition to the battlements. Despite the high number of affected components, more than 97% of cluster components, they only represent a small fraction of the classified 3D points in the

cluster. Similarly, for the cylindrical, mild transitions and medium curvature cluster, the reallocated components are located in the battlements and in some abrupt rocks distribution inside the curtain walls. In the case of the battlements, this behavior is caused due to their small size in relation to the curvature spherical vicinity used for the computation. However, due to the optimization protocol, they are moved to a cluster with crescent curvature in order to keep a higher spatial density. In the case of natural rocks aggrupation located in the wall, their curvature was lower than the threshold for the high curvature cluster (>0.4 m^{-1}). As result of the minimum area threshold, they were reallocated in the high curvature cluster since they were heterogeneously disposed in the curtain walls.
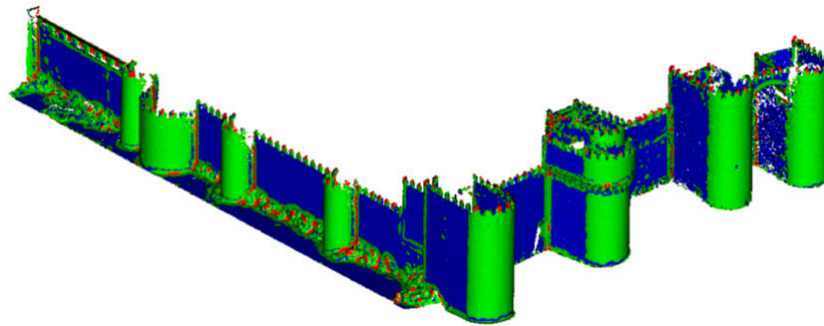

Figure 10. Initial MLS set of clusters: (i) planar or low curvature in blue; (ii) cylindrical, mild transitions and medium curvature in green; and (iii) the abrupt transitions of high curvature in red.

Table 6. Results of clustering refinement step (* the components are the result of the *curvature clustering* phase according to the main geometric elements of the CH site).

Cluster Curvature	Classification Legend	Initial Points	Components *	Reallocated Components	Reallocated Points	Final Points
Low	Blue	236,832	2022	1975 (97.7%)	13,716 (5.8%)	223,116
Medium	Green	263,580	1610	1563 (97.1%)	18,576 (7.0%)	258,720
High	Red	20,654	-	-	-	39,230

Finally, the weighted sampling is applied inside the clusters. For the low curvature, a resolution of 1 m is chosen, since the smooth process and plane-to-curve idealization. In the intermediate cluster, aimed for the towers, an arc to chord assimilation is applied. For a 50 cm chord, the idealization error will cause a sagittal of 13 mm for the worst case, which is inside the acceptable limits. Therefore, a 0.5 m weighted sampling is set. Lastly, the high curvature cluster is kept unmodified. The final point cloud has 58,476 points (Figure 11), which implies a reduction of 88.8% in relation to the spatially homogenized point cloud (521,090 points), and 94.1% in relation to the raw point cloud.
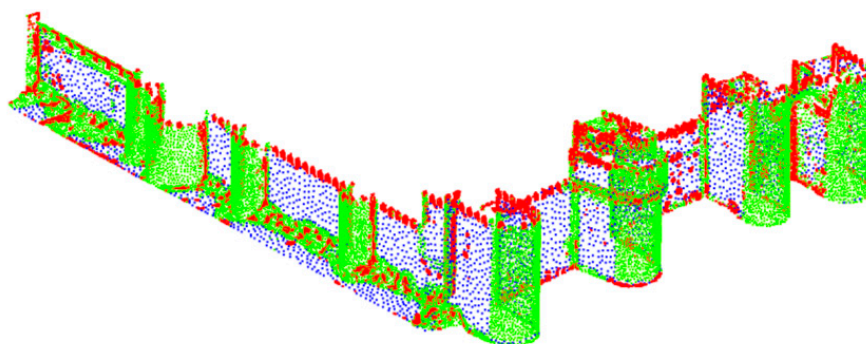

Figure 11. Final MLS point cloud optimization and simplification: (i) planar or low curvature in blue; (ii) cylindrical, mild transitions and medium curvature in green; and (iii) the abrupt transitions of high curvature in red.

5. Discussion

The novel use of MLS applied to the 3D surveying of large Cultural Heritage sites is evaluated and compared with the TLS, which is currently the most common technology used for this purpose.

MLS device combines different sensors on a mobile platform that allows obtaining an accurate and georeferenced 3D point cloud. Active sensors together with Inertial and Global Navigation System are synchronized in real time to collect and store data. The active sensor acquires detailed 3D points from a local coordinate system, while the IMU and GNSS systems provide and correct 3D points under a global reference frame. Moreover, some MLS can acquire RGB information captured by photographic or video cameras. Although the MLS spatial resolution depends on the active sensor (laser scanner) integrated on the mobile platform, usually the point clouds acquired by MLS cannot compete with TLS in terms of high resolution. Nevertheless, for large CH sites, the use of MLS could be more suitable, allowing the mapping of large and complex sites in an efficient way (e.g., historical cities or landscapes).

Otherwise, MLS reduces the data acquisition time thanks to the use of a mobile platform, while TLS needs multiple stations (sometimes even hundreds) to cover a large area. There are two main advantages of MLS technology compared to other 3D recording systems: (i) MLS is less expensive than airborne LiDAR systems boarded on airplanes or helicopters; and (ii) MLS can acquire accurate 3D data faster than TLS. On the contrary, its main disadvantage is that sometimes the transit with vans or cars is not possible due to conservation reasons or limitations of space (e.g., narrow streets). In this last case, it is possible to board the MLS on alternative platforms such as quads [62], backpack [16] or even autonomous robots [17].

MLS also reduces the data processing time in comparison with TLS, especially in large and complex CH sites. MLS directly produces a single point cloud, georeferenced with centimetric accuracy due to the IMU and GNSS calibrated sensors, whereas the 3D data captured by TLS have to be aligned in a relative or global reference system.

Finally, the visualization and management of large datasets still represent a bottleneck for both techniques (MLS and TLS). The ongoing development of 3D recording sensors and data capture technologies are advancing more rapidly than the management of large geometrical datasets. MLS and TLS usually produce massive point clouds (millions of points) requiring storage spaces of many GB. To advance this problem, 3D datasets (i.e., point clouds) need to be efficiently optimized and simplified for architectural and structural analysis (e.g., FEM), documentation and management (e.g., HBIM) or outreach purposes (e.g., Web Visualization). As additional benefits of the proposed point cloud optimization, the optimized point cloud will be improved for subsequent 3D modeling tasks based on meshing or reverse engineering procedures, improving the computational time and the resulting geometric definition.

In this paper, our main contribution was based on the use of algorithms and methodologies for the point cloud optimization, without any prior surface reconstruction. There are numerous algorithms to reduce the 3D point cloud in automatic way, but our approach was focused on an adaptive sampling that depends on the geometric features and also keeps the main structures without losing relevant details. The optimal solution was to find a compromise between the resolution acquired, the accuracy and the final size of the file, in order to obtain detailed 3D point clouds that could be stored, managed and visualized with a fluent real-time interaction.

6. Conclusions

This paper deals with a novel use of Mobile LiDAR System for the 3D recording of large Cultural Heritage sites. As part of the suitability assessment of this technology, an accuracy evaluation with a Terrestrial Laser Scanner was carried out. The obtained results, checked in an appropriate study case, allow us to confirm the suitability of Mobile LiDAR System techniques for 3D recording and modeling of large Cultural Heritage sites.

On the one hand, we were focused on time consumption. Comparing both 3D recording techniques, Mobile LiDAR System technology was a clear winner in terms of time used for data acquisition and data processing. Data coming from our study case shows that Mobile LiDAR System took only 1 h to sweep an area of 250,000 m^2 while the Terrestrial Laser Scanner took 159 h. This means considerable time saving.

On the other hand, spatial resolution was our concern. Terrestrial Laser Scanner could achieve a point cloud density of 15 mm (average of scanning distance: 20 m) while Mobile LiDAR System density was 60 mm (average of scanning distance: 25 m). In order to evaluate data accuracy of the Mobile LiDAR System, a comparison of both 3D point clouds was done, regarding the georeferencing error. Considering that the represented area involved a few kilometers, the results show that 95% of the MLS points acquired are inside of the tolerance range [−0.046 m; +0.047 m]. Even if Mobile LiDAR System provides a less dense point cloud, it is conclusive that it has enough spatial resolution and quality to provide the reconstruction of the most relevant architectural details in large Cultural Heritage sites.

In any case, due to the huge amount of acquired data, the final point clouds should be necessarily optimized for visualization and management purposes. A novel process for point cloud optimization is introduced to facilitate its handling by scholars from various disciplines. The proposed optimization methodology was based on a detail geometric analysis, allowing classifying the different structures into three main clusters (low, medium and high curvature). Different optimization parameters were used for each cluster according to their curvature, obtaining a reduced point cloud ca. 94.1% less in relation to the entire raw point cloud and guaranteeing an optimal solution for multiple purposes.

The results confirm that Mobile LiDAR System also shows more efficiency in terms of operation flexibility, acquisition and processing time, producing high quality and accurate data. However, shape complexity and surrounding characteristics, such as the environment location or the access restrictions, must be taken into account in further studies to define which is the best approach.

In the worst case, when the geometric complexity of the scene is high, the transit of vehicles is difficult or they are restricted access to the archaeological sites, the novel indoor LiDAR technologies (e.g., the backpack solution, mobile robots or the handheld LiDAR mapping system) could be used as an alternative outdoor solution.

To conclude, it would be interesting to extend our approach integrating different outdoors and indoors mobile techniques for large and complex Cultural Heritage sites.

Author Contributions: All of the authors conceived and designed the study. Pablo Rodríguez-Gonzálvez, Diego Gonzalez-Aguilera and Ángel Luis Muñoz-Nieto acquired the TLS data and processed it. Pedro Arias-Sanchez acquired the MLS data and processed it. Pablo Rodríguez-Gonzálvez and Belén Jiménez Fernández-Palacios implemented the methodology and analysed the results. Pablo Rodríguez-Gonzálvez, Belén Jiménez Fernández-Palacios and Diego Gonzalez-Aguilera wrote the manuscript and all authors read and approved the final version.

Conflicts of Interest: The authors declare no conflict of interest.

References

1. Guidi, G.; Micoli, L.L.; Gonizzi, S.; Brennan, M.; Frischer, B. Image-based 3D capture of cultural heritage artifacts an experimental study about 3D data quality. In Proceedings of the 2015 Digital Heritage, Granada, Spain, 28 September–2 October 2015; pp. 321–324.
2. Del Pozo, S.; Herrero-Pascual, J.; Felipe-García, B.; Hernández-López, D.; Rodríguez-Gonzálvez, P.; González-Aguilera, D. Multispectral radiometric analysis of façades to detect pathologies from active and passive remote sensing. *Remote Sens.* **2016**, *8*, 80. [CrossRef]

3. Borrmann, D.; Heß, R.; Houshiar, H.; Eck, D.; Schilling, K.; Nüchter, A. Robotic mapping of cultural heritage sites. *Int. Arch. Photogramm. Remote Sens. Spat. Inf. Sci.* **2015**, *XL-5/W4*, 9–16. [CrossRef]

4. Puente, I.; Solla, M.; González-Jorge, H.; Arias, P. NDT documentation and evaluation of the Roman Bridge of Lugo using GPR and mobile and static LiDAR. *J. Perform. Constr. Facil.* **2013**, *29*, 06014004. [CrossRef]

5. Casadio, F.; Daher, C.; Bellot-Gurlet, L. Raman spectroscopy of cultural heritage materials: Overview of applications and new frontiers in instrumentation, sampling modalities, and data processing. *Top. Curr. Chem.* **2016**, *374*, 62. [CrossRef] [PubMed]

6. Johnson, K.M.; Ouimet, W.B. Rediscovering the lost archaeological landscape of southern New England using airborne light detection and ranging (LiDAR). *J. Archaeol. Sci.* **2014**, *43*, 9–20. [CrossRef]

7. Von Schwerin, J.; Richards-Rissetto, H.; Remondino, F.; Spera, M.G.; Auer, M.; Billen, N.; Loos, L.; Stelson, L.; Reindel, M. Airborne LiDAR acquisition, post-processing and accuracy-checking for a 3D WebGIS of Copan, Honduras. *J. Archaeol. Sci. Rep.* **2016**, *5*, 85–104. [CrossRef]

8. Hyyppä, J.; Jaakkola, A.; Chen, Y.; Kukko, A. Unconventional LIDAR mapping from air, terrestrial and mobile. In *Photogrammetric Week, 2013*; Wichmann/VDE: Belin/Offenbach, Germany, 2013; pp. 205–214.

9. Puente, I.; González-Jorge, H.; Martínez-Sáchez, J.; Arias, P. Review of mobile mapping and surveying systems. *Measurement* **2013**, *46*, 2127–2145. [CrossRef]

10. Williams, K.; Olsen, M.; Roe, G.; Glennie, C. Synthesis of transportation applications of mobile LIDAR. *Remote Sens.* **2013**, *5*, 4652. [CrossRef]

11. Lim, S.; Thatcher, C.A.; Brock, J.C.; Kimbrow, D.R.; Danielson, J.J.; Reynolds, B.J. Accuracy assessment of a mobile terrestrial lidar survey at Padre Island National Seashore. *Int. J. Remote Sens.* **2013**, *34*, 6355–6366. [CrossRef]

12. Moskal, L.M.; Zheng, G. Retrieving forest inventory variables with terrestrial laser scanning (TLS) in urban heterogeneous forest. *Remote Sens.* **2012**, *4*, 1. [CrossRef]

13. González-Ferreiro, E.; Miranda, D.; Barreiro-Fernandez, L.; Bujan, S.; Garcia-Gutierrez, J.; Dieguez-Aranda, U. Modelling stand biomass fractions in Galician Eucalyptus globulus plantations by use of different LiDAR pulse densities. *For. Syst.* **2013**, *22*, 510–525. [CrossRef]

14. Bauwens, S.; Bartholomeus, H.; Calders, K.; Lejeune, P. Forest inventory with terrestrial LiDAR: A comparison of static and hand-held mobile laser scanning. *Forests* **2016**, *7*, 127. [CrossRef]

15. Zhang, S.; Wang, C.; Yang, Z.; Chen, Y.; Li, J. Automatic railway power line extraction using mobile laser scanning data. *Int. Arch. Photogramm. Remote Sens. Spat. Inf. Sci.* **2016**, *XLI-B5*, 615–619. [CrossRef]

16. Lauterbach, H.; Borrmann, D.; Heß, R.; Eck, D.; Schilling, K.; Nüchter, A. Evaluation of a backpack-mounted 3D mobile scanning system. *Remote Sens.* **2015**, *7*, 13753–13781. [CrossRef]

17. Ziparo, V.A.; Zaratti, M.; Grisetti, G.; Bonanni, T.M.; Serafin, J.; Cicco, M.D.; Proesmans, M.; Gool, L.V.; Vysotska, O.; Bogoslavskyi, I.; et al. Exploration and mapping of catacombs with mobile robots. In Proceedings of the 2013 IEEE International Symposium on Safety, Security, and Rescue Robotics, Linköping, Sweden, 21–26 October 2013; pp. 1–2.

18. Bosse, M.; Zlot, R.; Flick, P. Zebedee: Design of a spring-mounted 3-D range sensor with application to mobile mapping. *IEEE Trans. Robot.* **2012**, *28*, 1104–1119. [CrossRef]

19. Zlot, R.; Bosse, M.; Greenop, K.; Jarzab, Z.; Juckes, E.; Roberts, J. Efficiently capturing large, complex cultural heritage sites with a handheld mobile 3D laser mapping system. *J. Cult. Herit.* **2014**, *15*, 670–678. [CrossRef]

20. Sirmacek, B.; Shen, Y.; Lindenbergh, R.; Zlatanova, S.; Diakite, A. Comparison of Zeb1 and Leica C10 indoor laser scanning point clouds. *ISPRS Ann. Photogramm. Remote Sens. Spat. Inf. Sci.* **2016**, *III-1*, 143–149. [CrossRef]

21. Calisi, D.; Giannone, F.; Ventura, C.; Salonia, P.; Cottefoglie, F.; Ziparo, V.A. ARIS—A Robotic Approach to Digitization of Indoor and Underground Cultural Heritage Sites. In Proceedings of the International Congress on Digital Heritage, Granada, Spain, 28 September–2 October 2015.

22. Calisi, D.; Giannone, F.; Ventura, C.; Salonia, P.; Cottefoglie, F.; Ziparo, V.A. Digitizing Indoor and Underground Cultural Heritage Sites with Robots. *Sci. Res. Inf. Technol.* **2016**, *6*, 23–30.

23. Rondeau, M.-C. New Technologies for city asset mapping: Setting the standard in city digitalisation. *GeoInformatics* **2015**, *18*, 20–21.

24. Rönnholm, P.; Liang, X.; Kukko, A.; Jaakkola, A.; Hyyppä, J. Quality analysis and correction of mobile backpack laser scanning data. *ISPRS Ann. Photogramm. Remote Sens. Spat. Inf. Sci.* **2016**, *III-1*, 41–47. [CrossRef]

25. Sairam, N.; Nagarajan, S.; Ornitz, S. Development of mobile mapping system for 3D road asset inventory. *Sensors* **2016**, *16*, 367. [CrossRef] [PubMed]

26. Pauly, M.; Gross, M.; Kobbelt, L.P. Efficient simplification of point-sampled surfaces. In Proceedings of the Conference on Visualization, Boston, MA, USA, 27 October–1 November 2002; IEEE Computer Society: Boston, MA, USA, 2002; pp. 163–170.

27. Song, H.; Feng, H.-Y. A point cloud simplification algorithm for mechanical part inspection. In Proceedings of the Seventh International Conference on Information Technology for Balanced Automation Systems in Manufacturing and Services, Niagara Falls, ON, Canada, 4–6 September 2006; Shen, W., Ed.; Springer: Boston, MA, USA, 2006; pp. 461–468.

28. Charbonnier, P.; Tarel, J.-P.; Goulette, F. *On the Diagnostic of Road Pathway Visibility*; Transport Research Arena Europe: Bruxelles, France, 2010.

29. Yang, B.; Dong, Z. A shape-based segmentation method for mobile laser scanning point clouds. *ISPRS J. Photogramm. Remote Sens.* **2013**, *81*, 19–30. [CrossRef]

30. Sun, H.; Wang, C.; El-Sheimyb, N.; traffics Wang, P. Surrounding detection for terrestrial mobile mapping data quality evaluation. In Proceedings of the 6th International Symposium on Mobile Mapping Technology, São Paulo, Brazil, 21–24 July 2009.

31. Oude Elberink, S.; Khoshelham, K.; Arastounia, M.; Diaz Benito, D. Rail track detection and modelling in mobile laser scanner data. *ISPRS Ann. Photogramm. Remote Sens. Spat. Inf. Sci.* **2013**, *II-5/W2*, 223–228. [CrossRef]

32. Torres-Martínez, J.; Seddaiu, M.; Rodríguez-Gonzálvez, P.; Hernández-López, D.; González-Aguilera, D. A multi-data source and multi-sensor approach for the 3D reconstruction and web visualization of a complex archaelogical site: The case study of "Tolmo De Minateda". *Remote Sens.* **2016**, *8*, 550. [CrossRef]

33. Jiménez Fernández-Palacios, B.; Stefani, C.; Lombardo, J.; De Luca, L.; Remondino, F. Web visualization of complex reality-based 3D models with NUBES. In Proceedings of the IEEE Conference Digital Heritage 2013, Marseille, France, 28 October–1 November 2013; Volume 1, pp. 701–704.

34. Nubes Project. Available online: http://www.map.cnrs.fr/nubes/ (accessed on 25 December 2016).

35. Cultural Heritage Information System Project. Available online: http://lrv.ugr.es/chis/en/ (accessed on 25 December 2016).

36. Torres, J.C.; López, L.; Romo, C.; Arroyo, G.; Cano, P.; Lamolda, F.; Villafranca, M.M. Using a cultural heritage information system for the documentation of the restoration process. In Proceedings of the 2013 Digital Heritage, Marseille, France, 28 October–1 November 2013.

37. Von Schwerin, J.; Richards-Rissetto, H.; Agugiaro, G.; Remondino, F.; Girardi, G. QueryArch3D: A 3D WebGIS System linking 3D visualizations to archaeological data. In Proceedings of the Computer Applications and Quantitative Methods in Archaeology, Southampton, UK, 26–30 March 2012.

38. Prandi, F.; Devigili, F.; Soave, M.; Di Staso, U.; De Amicis, R. 3D web visualization of huge cityGML models. *Int. Arch. Photogramm. Remote Sens. Spat. Inf. Sci.* **2015**, *XL-3/W3*, 601–605. [CrossRef]

39. Conforti, D.; Zampa, F. Lynx mobile mapper for surveying city centers and highways. *Int. Arch. Photogramm. Remote Sens. Spat. Inf. Sci.* **2011**, *XXXVIII-5/W16*, 219–222. [CrossRef]

40. Hofmann, S.; Brenner, C. Accuracy assessment of mobile mapping point clouds using the existing environment as terrestrial reference. *Int. Arch. Photogramm. Remote Sens. Spat. Inf. Sci.* **2016**, *XLI-B1*, 601–608. [CrossRef]

41. Chan, T.O. Feature-Based Boresight Self-Calibration of a Mobile Mapping System. Master's Thesis, University of Calgary, Calgary, AB, Canada, 2012.

42. Grussenmeyer, P.; Landes, T.; Doneus, M.; Lerma, J. Basics of range-based modelling techniques in cultural heritage 3D recording. In *3D Recording, Documentation and Management of Cultural Heritage*; Whittles Publishing: Dunbeath, UK, 2016.

43. Schulz, T. Calibration of a Terrestrial Laser Scanner for Engineering Geodesy. Ph.D. Thesis, Technical University of Berlin, Berlin, Germany, 2007.

44. Remondino, F. Heritage recording and 3D modeling with photogrammetry and 3D scanning. *Remote Sens.* **2011**, *3*, 1104–1138. [CrossRef]

45. Gonzalez-Jorge, H.; Rodriguez-Gonzalvez, P.; Gonzalez-Aguilera, D.; Varela-Gonzalez, M. Metrological comparison of terrestrial laser scanning systems Riegl LMS Z390i and Trimble GX. *Opt. Eng.* **2011**, *50*, 116201–116209.

46. González-Aguilera, D.; Rodríguez-Gonzálvez, P.; Armesto, J.; Arias, P. Trimble GX200 and Riegl LMS-Z390i sensor self-calibration. *Opt. Express* **2011**, *19*, 2676–2693. [CrossRef] [PubMed]

47. Besl, P.J.; McKay, N.D. A method for registration of 3-d shapes. *IEEE Trans. Pattern Anal. Mach. Intell.* **1992**, *14*, 239–256. [CrossRef]

48. Tombari, F.; Salti, S.; Di Stefano, L. Performance evaluation of 3D keypoint detectors. *Int. J. Comput. Vis.* **2013**, *102*, 198–220. [CrossRef]

49. Akca, D. Full automatic registration of laser scanner point clouds. In Proceedings of the Optical 3-D Measurement Techniques VI, Zurich, Switzerland, 22–25 September 2003; pp. 330–337.

50. Paparoditis, N.; Papelard, J.-P.; Cannelle, B.; Devaux, A.; Soheilian, B.; David, N.; Houzay, E. Stereopolis II: A multi-purpose and multi-sensor 3D mobile mapping system for street visualisation and 3D metrology. *Rev. Fr. Photogramm. Télédétec.* **2012**, *200*, 69–79.

51. Toschi, I.; Rodríguez-Gonzálvez, P.; Remondino, F.; Minto, S.; Orlandini, S.; Fuller, A. Accuracy evaluation of a mobile mapping system with advanced statistical methods. *Int. Arch. Photogramm. Remote Sens. Spat. Inf. Sci.* **2015**, *XL-5/W4*, 245–253. [CrossRef]

52. Lague, D.; Brodu, N.; Leroux, J. Accurate 3D comparison of complex topography with terrestrial laser scanner: Application to the Rangitikei canyon (N-Z). *ISPRS J. Photogramm. Remote Sens.* **2013**, *82*, 10–26. [CrossRef]

53. Höhle, J. The assessment of the absolute planimetric accuracy of airborne lasers canning. *Int. Arch. Photogramm. Remote Sens. Spat. Inf. Sci.* **2011**, *XXXVIII-5/W12*, 145–150.

54. Rodríguez-Gonzálvez, P.; Garcia-Gago, J.; Gomez-Lahoz, J.; González-Aguilera, D. Confronting passive and active sensors with non-gaussian statistics. *Sensors* **2014**, *14*, 13759–13777. [CrossRef] [PubMed]

55. Cloud Compare v.2.7.0. Available online: www.danielgm.net/cc/ (accessed on 7 October 2016).

56. Rodríguez-Gonzálvez, P.; González-Aguilera, D.; Hernández-López, D.; González-Jorge, H. Accuracy assessment of airborne laser scanner dataset by means of parametric and non-parametric statistical methods. *IET Sci. Meas. Technol.* **2015**, *9*, 505–513. [CrossRef]

57. Levin, D. The approximation power of moving least-squares. *Math. Comput. Am. Math. Soc.* **1998**, *67*, 1517–1531. [CrossRef]

58. Serna, M. Walls: Speaking of Towers, Battlements, Gates. *Diario de Ávila*, 13 October 2002.

59. Mancera-Taboada, J.; Rodríguez-Gonzálvez, P.; González-Aguilera, D.; Muñoz-Nieto, Á.; Gómez-Lahoz, J.; Herrero-Pascual, J.; Picón-Cabrera, I. On the use of laser scanner and photogrammetry for the global digitization of the medieval walls of Avila. *Int. Arch. Photogramm. Remote Sens. Spat. Inf. Sci.* **2010**, *XXXVIII*, 169–174.

60. Haala, N.; Peter, M.; Cefalu, A.; Kremer, J. Mobile lidar mapping for urban data capture. In Proceedings of the 14th International Conference on Virtual Systems and Multimedia, Limassol, Cyprus, 20–25 October 2008; pp. 95–100.

61. Rodríguez-Gonzálvez, P.; Nocerino, E.; Menna, F.; Minto, S.; Remondino, F. 3D surveying & modeling of underground passages in WWI fortifications. *Int. Arch. Photogramm. Remote Sens. Spat. Inf. Sci.* **2015**, *XL-5/W4*, 17–24.

62. Kurkin, A.; Pelinovsky, E.; Tyugin, D.; Kurkina, O.; Belyakov, V.; Makarov, V.; Zeziulin, D. Coastal remote sensing using unmanned ground vehicles. *Int. J. Environ. Sci.* **2016**, *1*, 183–189.